

# 1 ENSO-conditioned evolution of global mean surface 2 temperature

3 Michael K. Tippett<sup>1</sup> and Emily J. Becker<sup>2</sup>

4 <sup>1</sup>Department of Applied Physics and Applied Mathematics, Columbia University, New York, New York

5 <sup>2</sup>Rosenstiel School of Marine, Atmospheric, and Earth Science, University of Miami, Miami, Florida

## 6 Key Points:

- 7 • A simple regression model was developed to represent the delayed response of global  
8 mean surface temperature to ENSO
- 9 • The model associates a 1°C December Niño-3.4 anomaly with global mean tem-  
10 perature increases of 0.03°C in summer and 0.11°C in late winter
- 11 • Initialized climate forecasts show similar ENSO-temperature links and provide  
12 additional predictive value prior to the ENSO peak

## Abstract

Here we examined how the June–May trajectory of global mean surface temperature (GMST) can be anticipated from recent GMST evolution and upcoming boreal winter Niño-3.4 values. Principal component analysis and dimension reduction of the data led to a simple, interpretable model in which the June–May monthly GMST trajectory is conditioned on two quantities: the average GMST of the prior 12 months and the upcoming December value of Niño-3.4. Including ENSO improves performance relative to persistence baselines that do not include ENSO, especially during the time of the year when atmospheric bridge mechanisms are active. The model associates a December Niño-3.4 anomaly of  $1^{\circ}\text{C}$  with a GMST increase of about  $0.03^{\circ}\text{C}$  during June–August followed by a peak increase of about  $0.11^{\circ}\text{C}$  in the following February. In comparison, initialized climate forecasts show broadly similar ENSO–GMST relationships and provide additional skill prior to the ENSO peak.

## Plain Language Summary

Global mean surface temperature (GMST) is changing due to anthropogenic and natural forcing, as well as natural variability, with El Niño–Southern Oscillation (ENSO) being the dominant component of year-to-year natural variability. In this study, we examined how the June-to-May evolution of global mean temperature can be anticipated from two pieces of information available near the beginning of June: the recent GMST level and the expected state of ENSO over the same June-to-May period. In a statistical model, a December Niño-3.4 anomaly of  $1^{\circ}\text{C}$  is preceded by a GMST increase of about  $0.03^{\circ}\text{C}$  during June–August and followed by an increase of about  $0.11^{\circ}\text{C}$  in February. Initialized climate forecasts show similar links between ENSO and global mean temperature and add more information before the ENSO peak.

## 1 Introduction

Global mean surface temperature (GMST) is trending upward due to human-caused increases in greenhouse gases. Superimposed on this upward trend are short-term GMST variations in response to natural forcing (e.g., volcanoes) and internal variability. ENSO is the dominant component of internal variability on seasonal timescales, and its influence on GMST is well established (e.g., Angell, 1981; Trenberth et al., 2002). During warm ENSO conditions (El Niño), GMST tends to be elevated relative to the long-term trend,

44 while during cool ENSO conditions (La Niña), the opposite tends to occur. The increase  
45 in GMST from a strong El Niño can be substantial. Lean and Rind (2008) attributed  
46 about 0.23°C of GMST warming to the 1997 “super” El Niño. More recently, the World  
47 Meteorological Organization noted, “The most recent El Niño, in 2023–24, was one of  
48 the five strongest on record and it played a role in the record global temperatures we saw  
49 in 2024” (Raghuraman et al., 2024; World Meteorological Organization, 2026).

50 Tippett and Becker (2024) compared long-lead forecasts of monthly GMST from  
51 the North American Multi-Model Ensemble (NMME; Becker et al., 2022; Kirtman et al.,  
52 2014) to a simple linear trend. The useful skill (i.e., better than the linear trend) of NMME  
53 forecasts targeting May–August was limited to lead times of only a month or two, while  
54 forecasts targeting boreal winter months had useful skill as far as 12 months ahead. The  
55 dependence of GMST forecast skill on target month and lead time is reminiscent of the  
56 ENSO spring predictability barrier. Consistent with that interpretation, when ENSO was  
57 removed from NMME forecasts of GMST, most of their useful skill was removed as well,  
58 evidence that ENSO was a primary source of skill (Tippett & Becker, 2024).

59 However, even from an observational perspective, the timing and amplitude of the  
60 ENSO influence on monthly GMST remain poorly quantified. For example, given the  
61 evolution of an ENSO event, there is no clear quantitative description of the associated  
62 month-by-month evolution of GMST. One reason for this gap is that previous GMST–  
63 ENSO studies (e.g., Trenberth et al., 2002) have often pooled all months together in their  
64 analysis, which obscures the seasonal structure of both ENSO and its influence on GMST.  
65 Another reason is that the goal of many studies was to remove ENSO-related variabil-  
66 ity from GMST in order to better isolate trends and responses to external forcing (Angell,  
67 2000; Lean & Rind, 2008; Foster & Rahmstorf, 2011). For that purpose, they focused  
68 on the lag at which the ENSO–GMST correlation is strongest, leaving open the broader  
69 question of how ENSO influences the month-by-month evolution of GMST.

70 This inability to translate ENSO information into GMST responses prevents the  
71 operational ENSO predictions produced monthly by forecast centers worldwide from be-  
72 ing used to anticipate GMST. In early 2026, forecasts of a strong El Niño have led to  
73 speculation that it could boost GMST by about 0.2°C (e.g., Keith-Lucas, 2026). While  
74 this estimate appears plausible, exactly how a given forecast of ENSO conditions trans-

lates into an expected GMST anomaly is less clear, both in terms of timing and amplitude.

Here, we addressed this gap by deriving a simple and interpretable regression model that outputs GMST evolution at monthly resolution over a June–May 12-month period, given a forecast of ENSO conditions over the same period. The June–May period was chosen because it approximates the typical ENSO development and decay cycle and because ENSO forecasts initialized after boreal spring have useful skill through the following winter (e.g., L’Heureux et al., 2020). We derived the regression model using observed ENSO evolution, analogous to the perfect-prog framework in model output statistics (Glahn & Lowry, 1972; W. H. Klein et al., 1959). We then used initialized climate forecasts in two ways. First, we used forecast ENSO information as input to the regression model, allowing us to assess the effect of replacing observed ENSO evolution with forecast ENSO evolution. Second, we used initialized climate forecasts as a dynamical comparison. This comparison allowed us to assess whether the ENSO–GMST relationships in the forecasts resemble those inferred from observations, and whether direct initialized forecasts of GMST provide additional predictive information beyond the regression model.

Data sources and methods are described in Section 2. Section 3 develops the regression model, evaluates its performance, and compares it with initialized climate forecasts. A summary and discussion are given in Section 4.

## 2 Data and Methods

We used monthly data from June 1979 through May 2026, comprising 47 June–May ENSO years. Global mean surface temperature (GMST) was computed as the area-weighted global mean of gridded surface temperature from NOAAGlobalTemp v6.1.0 (Huang et al., 2022). NOAAGlobalTemp uses the current WMO climatological standard normals period, 1991–2020, as the reference period for temperature anomalies. Its 1850–1900 mean is  $-0.78^{\circ}\text{C}$ , and this value was subtracted to form preindustrial anomalies. The Niño-3.4 index was computed from ERSSTv5 (Huang et al., 2017a) as the area-weighted sea surface temperature over  $5^{\circ}\text{S}$ – $5^{\circ}\text{N}$ ,  $170^{\circ}\text{W}$ – $120^{\circ}\text{W}$ . Anomalies are relative to the 1991–2020 base period. We also made limited use of the relative Niño-3.4 index (L’Heureux et al., 2024).

105 Forecasts of monthly GMST and the Niño-3.4 index were taken from the North Amer-  
106 ican Multi-Model Ensemble (NMME) database (Kirtman et al., 2014; Becker et al., 2022).  
107 We used 1 June initialized forecasts from the seven models currently producing real-time  
108 forecasts: COLA-RSMAS-CCSM4, COLA-RSMAS-CESM1, CanESM5, GEM5.2-NEMO,  
109 GFDL-SPEAR (intermittently available after May 2025), NASA-GEOSS2S, and NCEP-  
110 CFSv2. Start dates cover 1 June 1991–1 June 2026. Most forecasts extend 12 months  
111 beyond their start date; NASA-GEOSS2S and NCEP-CFSv2 forecasts extend nine and  
112 ten months, respectively. The multi-model mean was computed by averaging the ensem-  
113 ble means from each model, and the multi-model ensemble consists of all ensemble mem-  
114 bers from all models. Two-period forecast climatologies were used to compute Niño-3.4  
115 anomalies in COLA-RSMAS-CCSM4, COLA-RSMAS-CESM1, and NCEP-CFSv2 fore-  
116 casts (Barnston et al., 2019).

117 Principal component analysis (PCA) was applied to observed monthly anomalies  
118 of Niño-3.4 and GMST arranged as  $12 \times 47$  matrices, with rows corresponding to months  
119 and columns to June–May years. Double-centered PCA was applied to the same matri-  
120 ces after also removing June–May means (column averages). We used the convention that  
121 principal components (PCs) have unit variance and empirical orthogonal functions (EOFs)  
122 carry physical units (DelSole & Tippett, 2022). Reconstructions were formed as prod-  
123 ucts of EOFs and PCs, with removed means added back.

124 Coefficient of determination ( $R^2$ ), root-mean-square error (RMSE), and mean-squared-  
125 error skill score (MSESS) were used as summary measures of regression model perfor-  
126 mance (Wilks, 2011). Statistical significance of differences in RMSE was assessed using  
127 the Wilcoxon signed-rank and sign tests applied to paired squared errors. Because the  
128 RMSE values were computed using the same GMST data, RMSE values for different mod-  
129 els are not independent, and an  $F$ -test for equality of variances is inappropriate (DelSole  
130 & Tippett, 2014).

### 131 **3 Results**

132 We used a regression framework to quantify the dependence of GMST evolution  
133 on ENSO, with ENSO represented by the Niño-3.4 index. We represented evolution us-  
134 ing 12-month June–May sequences (trajectories) of GMST and Niño-3.4 values. We ac-  
135 counted for the GMST trend in an autoregressive manner by conditioning on prior val-

136 ues of GMST rather than including explicit time trends or radiative forcing. This ap-  
 137 proach is appropriate here because the primary goal is to quantify the dependence of GMST  
 138 on ENSO, in contrast to studies that focus on trend estimation or the separation of forced  
 139 and internal variability. This formulation can be expressed as the vector equation:

$$\begin{bmatrix} \text{GMST}_{\text{Jun}} \\ \text{GMST}_{\text{Jul}} \\ \vdots \\ \text{GMST}_{\text{Apr}} \\ \text{GMST}_{\text{May}} \end{bmatrix} (y+1) = \mathbf{A}_{12} \begin{bmatrix} \text{GMST}_{\text{Jun}} \\ \text{GMST}_{\text{Jul}} \\ \vdots \\ \text{GMST}_{\text{Apr}} \\ \text{GMST}_{\text{May}} \end{bmatrix} (y) + \mathbf{B}_{12} \begin{bmatrix} \text{Niño-3.4}_{\text{Jun}} \\ \text{Niño-3.4}_{\text{Jul}} \\ \vdots \\ \text{Niño-3.4}_{\text{Apr}} \\ \text{Niño-3.4}_{\text{May}} \end{bmatrix} (y+1), \quad (1)$$

141 where  $y$  indexes June–May years, and the  $12 \times 12$  coefficient matrices  $\mathbf{A}_{12}$  and  $\mathbf{B}_{12}$  rep-  
 142 resent, respectively, the dependence of a GMST trajectory on its prior values and on the  
 143 contemporaneous Niño-3.4 trajectory. In addition to quantifying the dependence of GMST  
 144 on ENSO, this model can be used in a predictive manner to anticipate GMST evolution  
 145 given a forecast Niño-3.4 trajectory.

146 The regression model in (1) is high-dimensional with 24 predictors and 12 predic-  
 147 tand. The matrices  $\mathbf{A}_{12}$  and  $\mathbf{B}_{12}$  together contain 288 coefficients. To avoid overfitting,  
 148 facilitate interpretation, and reduce the complexity of the model, we applied PCA to the  
 149 two datasets. PCA is an unsupervised and systematic dimension-reduction method that  
 150 optimizes explained variance and, as used here, ignores relationships between predictors  
 151 and predictands. Previous work found that 12-month Niño-3.4 trajectories are well ap-  
 152 proximated by one or two PCs, both in observations and in seasonal forecasts (Bunge  
 153 & Clarke, 2009; Tippett & L’Heureux, 2020). Consistent with those results, we found  
 154 that approximately 95% of the variability of June–May Niño-3.4 segments is explained  
 155 by the first two PCs (Fig. 1a). Moreover, the same is true of GMST—approximately 95%  
 156 of the variability of a June–May GMST trajectory is explained by the first two PCs (Fig.  
 157 1b).

158 Although PCA need not yield physically meaningful or readily explainable com-  
 159 ponents, the leading PCs of GMST and Niño-3.4 trajectories admit relatively clear in-  
 160 terpretations. EOF1 of Niño-3.4 peaks in December, reflecting the seasonal phase lock-  
 161 ing of ENSO (Fig. 1a). EOF2 of Niño-3.4 is a dipole in time centered on December. The  
 162 dipole structure is related to the mathematical requirement that EOF2 be orthogonal

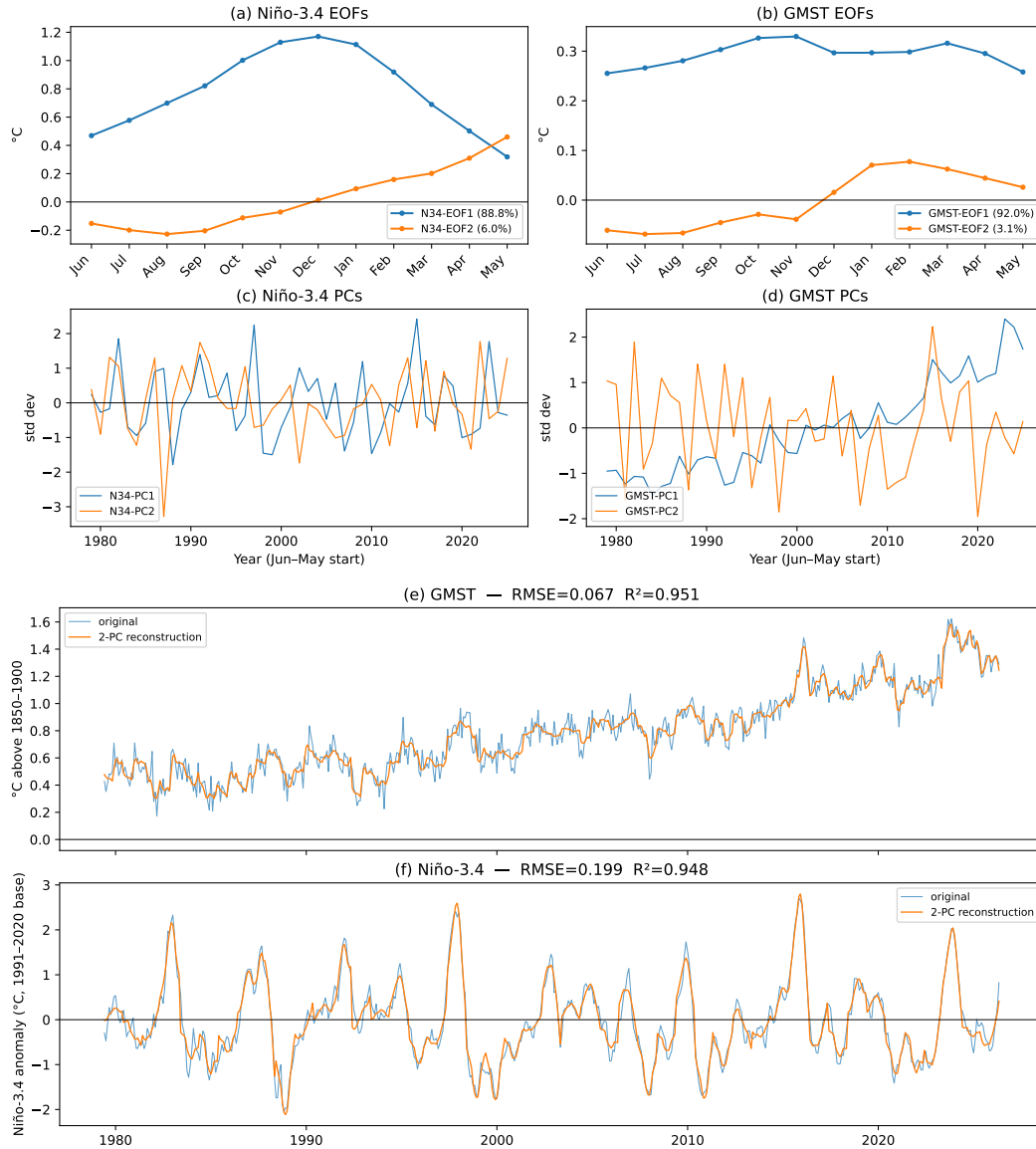


**Figure 1.** The leading two EOFs of June–May trajectories of (a) Niño-3.4 and (b) global mean surface temperature (GMST). The corresponding leading two PCs of (c) Niño-3.4 and (d) GMST. Two-PC reconstructions of (e) Niño-3.4 and (f) GMST with root-mean-squared error (RMSE) and  $R^2$  values in the title.

163 to EOF1 and serves to represent features such as shifts of the Niño-3.4 peak and ENSO  
 164 events that persist longer or decay more rapidly. EOF1 of GMST is nearly uniform across  
 165 months (Fig. 1b) and its PC has a clear upward trend (Fig. 1d); together they represent  
 166 a nearly month-independent warming trend. EOF2 of GMST is negative and roughly  
 167 uniform over the June–November period until it rises in December and peaks in January  
 168 and February, while PC2 shows no visible trend. The asymmetry of the dipole structure  
 169 of EOF2 suggests that it represents the delayed post-peak response of GMST to ENSO  
 170 via the atmospheric bridge (Alexander et al., 2002; S. A. Klein et al., 1999). Reconstruc-  
 171 tions of Niño-3.4 and GMST show that two EOFs are adequate to capture interannual  
 172 variability ( $R^2$  values of about 95%; Fig. 1e, f), although more unresolved subannual vari-  
 173 ability is visible in the GMST time series than in the Niño-3.4 time series because much  
 174 of the GMST variance is associated with its long-term trend.

175 The PCA analysis motivates replacing (1) with the four-PC model:

$$176 \begin{bmatrix} \text{GMST-PC1} \\ \text{GMST-PC2} \end{bmatrix} (y+1) = \mathbf{A}_{4\text{PC}} \begin{bmatrix} \text{GMST-PC1} \\ \text{GMST-PC2} \end{bmatrix} (y) + \mathbf{B}_{4\text{PC}} \begin{bmatrix} \text{N34-PC1} \\ \text{N34-PC2} \end{bmatrix} (y+1), \quad (2)$$

177 where the  $2 \times 2$  matrices  $\mathbf{A}_{4\text{PC}}$  and  $\mathbf{B}_{4\text{PC}}$  represent, respectively, the dependence of  
 178 the first two PCs of GMST on their prior values and on the contemporaneous values of  
 179 PC1 and PC2 of Niño-3.4. The number of coefficients is now reduced from 288 to eight.

180 We next examined the simultaneous and lagged correlations of the first two PCs  
 181 of Niño-3.4 and GMST. The strongest simultaneous correlation is the 0.61 correlation  
 182 between N34-PC1 and GMST-PC2, which supports our hypothesis that GMST-EOF2  
 183 represents the delayed GMST response to ENSO (Fig. 2a). The other simultaneous cor-  
 184 relations are weak ( $R^2 < 4\%$ ). The strongest lagged relation between PCs is the 0.92  
 185 correlation between GMST-PC1( $y$ ) and GMST-PC1( $y+1$ ), which reflects the upward  
 186 trend in GMST-PC1 and the resulting strong year-to-year persistence (Fig. 2b). In con-  
 187 trast, the lag-1 autocorrelation of GMST-PC2 is small and negative ( $r = -0.18$ ), con-  
 188 sistent with the interpretation of GMST-PC2 as an ENSO response with little persis-  
 189 tence from one year to the next. The source of the correlation between N34-PC2( $y$ ) and  
 190 N34-PC1( $y+1$ ) is less clear, though it is visually evident in the PC time series (Fig.  
 191 1c). It might reflect imperfect alignment of the June–May year with the ENSO life cy-  
 192 cle. The correlation between N34-PC2( $y$ ) and GMST-PC2( $y+1$ ) ( $r = 0.36$ ) is explained  
 193 almost entirely by the pathway N34-PC2( $y$ )  $\rightarrow$  N34-PC1( $y+1$ )  $\rightarrow$  GMST-PC2( $y+$

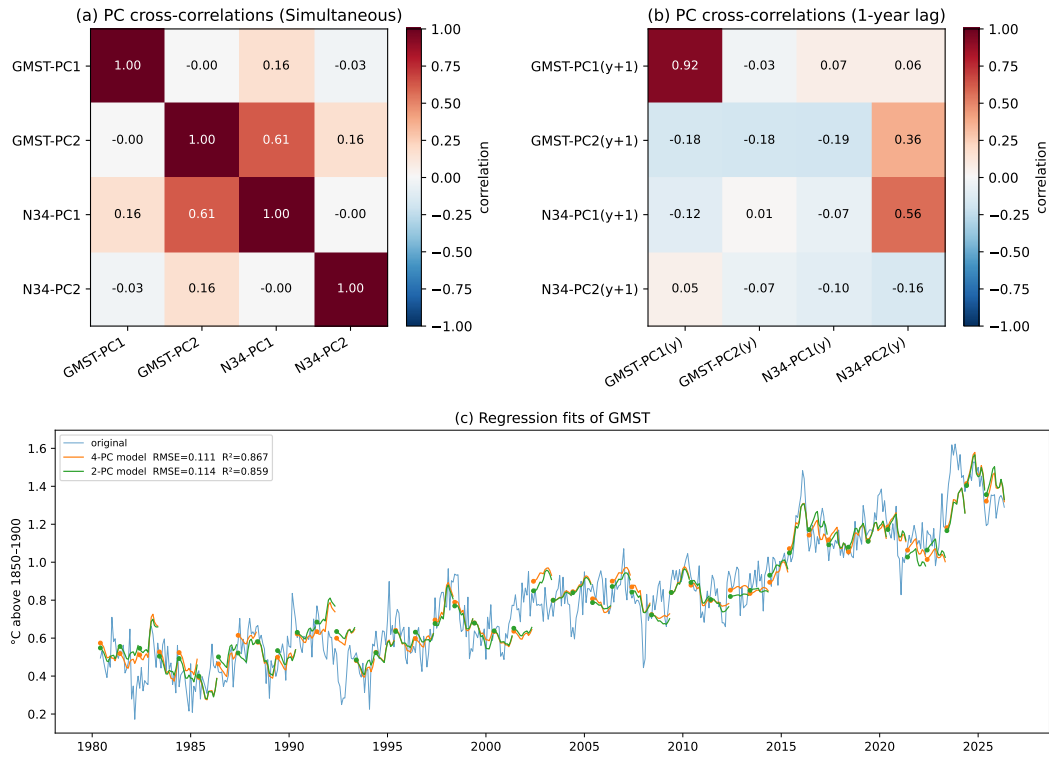


**Figure 2.** (a) Simultaneous and (b) one-year lag correlations between the first two PCs of Niño-3.4 and global mean surface temperature (GMST). Panel (c) shows the GMST time series and its fit by the four-PC and two-PC models (see text for model details). Dots indicate June–May segment starts. Model RMSE and  $R^2$  are shown in the legend.

194 1). After accounting for N34-PC1( $y+1$ ), the partial correlation between N34-PC2( $y$ )  
 195 and GMST-PC2( $y+1$ ) is only 0.03.

196 The correlation analysis above suggests that little is lost by using only two PCs as  
 197 predictors: GMST-PC1( $y$ ) and N34-PC1( $y+1$ ). The two-PC model is:

$$198 \begin{bmatrix} \text{GMST-PC1} \\ \text{GMST-PC2} \end{bmatrix} (y+1) = \mathbf{A}_{2\text{-PC}} \text{GMST-PC1}(y) + \mathbf{B}_{2\text{-PC}} \text{N34-PC1}(y+1), \quad (3)$$

199 where the  $2 \times 1$  matrices  $\mathbf{A}_{2\text{-PC}}$  and  $\mathbf{B}_{2\text{-PC}}$  represent, respectively, the dependence of  
 200 the first two PCs of GMST on the prior value of PC1 of GMST and on the contempo-  
 201 raneous value of PC1 of Niño-3.4. The number of coefficients is reduced from eight to  
 202 four. The fit obtained with these two predictors is nearly identical to that obtained with  
 203 four predictors (Fig. 2c), consistent with only the coefficients of GMST-PC1( $y$ ) and N34-  
 204 PC1( $y+1$ ) being large and statistically significant in the four-predictor model (Table  
 205 S1) and their having nearly the same values in the two-predictor model (Table S2).

206 While the two-PC predictor model is effective and parsimonious, further simpli-  
 207 fications can improve interpretability. In particular, the predictors GMST-PC1( $y$ ) and  
 208 N34-PC1( $y+1$ ) are defined by the PCA itself and depend on the specific data used. Re-  
 209 placing the predictor PCs with quantities that closely approximate them, but whose cal-  
 210 culation is more transparent, would yield a more explainable model. Because N34-PC1  
 211 is highly correlated ( $r > 0.98$ ) with the December Niño-3.4 value (Fig. 3a), we replaced  
 212 N34-PC1 with December Niño-3.4. This close correspondence follows from the structure  
 213 of the leading EOFs: EOF1 peaks in December, while EOF2 is close to zero in Decem-  
 214 ber. We replaced GMST-PC1 with the June–May mean GMST, which we refer to as the  
 215 GMST level. The GMST level is highly correlated with GMST-PC1 ( $r > 0.99$ ; Fig. 3b)  
 216 because GMST-EOF1 is nearly uniform across months. This replacement suggests an  
 217 alternative decomposition of GMST in which the first component is simply the level (June–  
 218 May mean), and the second component captures as much as possible of the remaining  
 219 variance. We implemented this idea by decomposing each June–May GMST trajectory  
 220 into its June–May level and departures from that level, and then applying PCA to the  
 221 departures. Because this decomposition removes both monthly means and June–May means,  
 222 we call it double-centered PCA (DC-PCA). Although DC-PCA is not variance-optimal,  
 223 the loss is small: the variance explained by the first two modes decreases from 95.1% to  
 224 94.6% (Fig. S1). The leading EOF from the double-centered decomposition is similar to

225 GMST-EOF2 (Fig. 3b), and GMST-DC-PC1 is also similar to GMST-PC2, with cor-  
 226 relation 0.992 (Fig. 3b).

227 These replacements (N34-PC1 replaced by December Niño-3.4 and GMST-PC1 re-  
 228 placed by level) give the simplified model:

$$229 \begin{bmatrix} \text{GMST}_{\text{level}} \\ \text{GMST-DC-PC1} \end{bmatrix} (y + 1) = \mathbf{A} \text{GMST}_{\text{level}}(y) + \mathbf{B} \text{Niño-3.4}_{\text{Dec}}(y + 1), \quad (4)$$

230 where the  $2 \times 1$  matrices  $\mathbf{A}$  and  $\mathbf{B}$  represent, respectively, the dependence of the GMST  
 231 level and GMST-DC-PC1 on the prior value of the GMST level and on the contempo-  
 232 raneous December value of Niño-3.4 (regression summary in Table S3). The performance  
 233 of the simplified model is nearly identical to that of the two-PC predictor model (Fig.  
 234 3c).

235 An attractive feature of the simplified model is that, once the recent GMST level  
 236 is specified, the shape of the predicted GMST response is fixed and only its amplitude  
 237 changes with the December Niño-3.4 value. Figure 3d shows the implied June–May GMST  
 238 response per  $+1^\circ\text{C}$  of December Niño-3.4. The response is about  $0.03^\circ\text{C}$  during June–  
 239 August, rises sharply beginning in December, and peaks at about  $0.11^\circ\text{C}$  in February.  
 240 The same analysis using relative Niño-3.4 gives a similar GMST response (Fig. 3d), in-  
 241 dicated that the result is not sensitive to the choice of ENSO index. The slightly weaker  
 242 response obtained with relative Niño-3.4 reflects its larger December variance during this  
 243 period—about 8% greater than that of the traditional Niño-3.4 index—rather than weaker  
 244 correlation with GMST residuals (Fig. S2; Table S4). The simplified model allows state-  
 245 ments of the form: “given the recent 12-month average of GMST and the expected De-  
 246 cember Niño-3.4 value, the June–May GMST trajectory is expected to be ...”. Specif-  
 247 ically, the observed June 2025–May 2026 GMST level of  $1.3^\circ\text{C}$  and an NMME-forecast  
 248 December 2026 Niño-3.4 value of  $+3.3^\circ\text{C}$  gives a predicted February 2027 peak near  $1.6^\circ\text{C}$   
 249 above preindustrial (Fig. 3e). For comparison, we show the NMME GMST forecast (June  
 250 2026 initialization) whose values peak near  $1.75^\circ\text{C}$ .

251 Having derived the simplified regression model, we next addressed three important  
 252 questions:

- 253 • How much is gained by accounting for ENSO?
- 254 • How much does performance change when forecast rather than observed Decem-  
 255 ber Niño-3.4 is used?

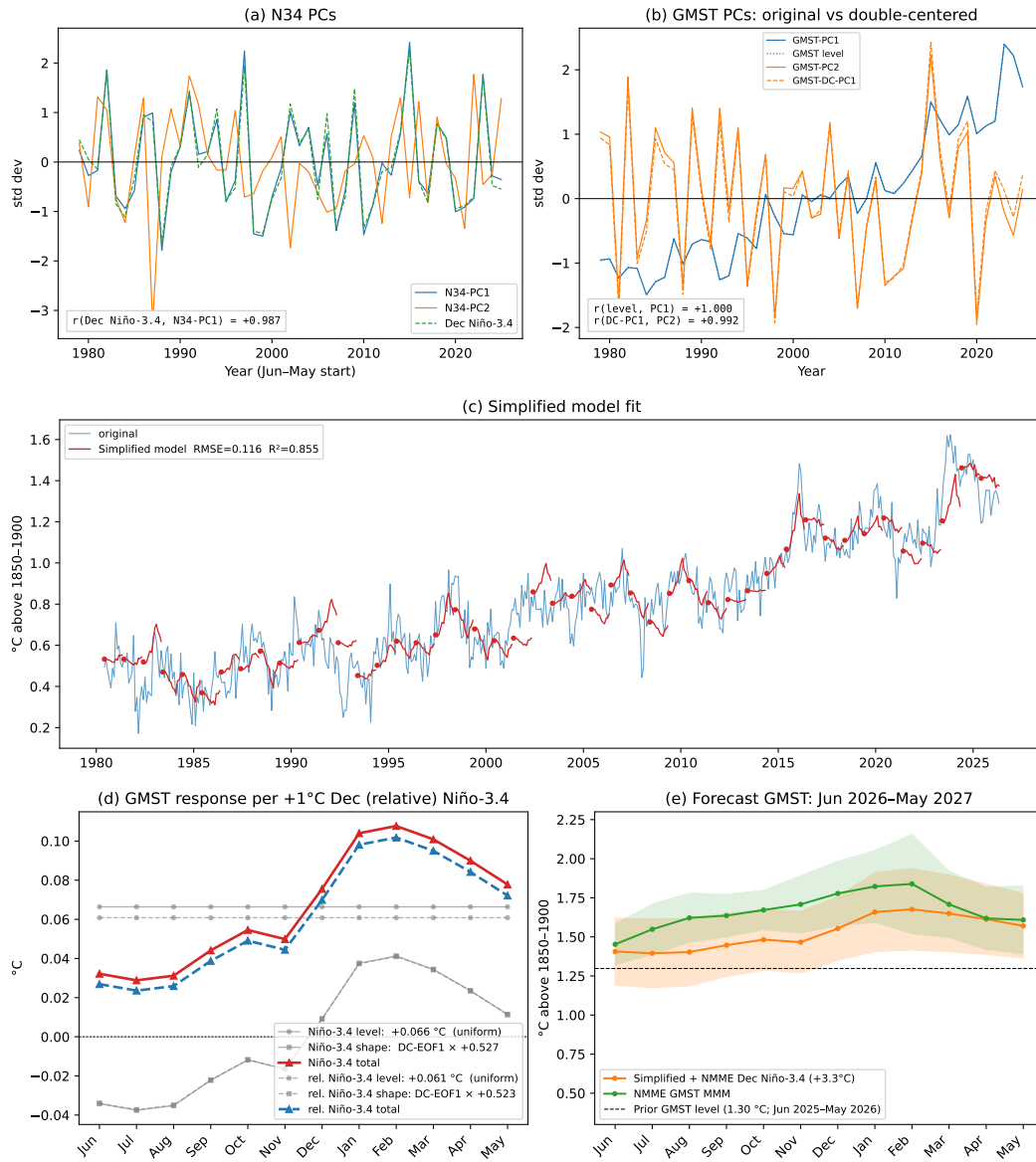


**Figure 3.** Comparisons of (a) N34-PC1 with December Niño-3.4 and (b) GMST PCs with GMST level and GMST-DC-PC1. Panel (c) shows the GMST time series and its fit by the simplified model (see text for details). Panel (d) shows the implied June–May GMST response per +1°C of December Niño-3.4 and relative Niño-3.4. Panel (e) shows NMME ( $\pm 2$  std shading) and simplified model (95% prediction interval) forecasts of June 2026–May 2027 GMST

- How does the simplified regression model compare with initialized climate forecasts of GMST?

This comparison helps to determine whether the simplified statistical model captures information already represented in dynamical forecasts, or whether the dynamical forecasts provide additional predictive information. To address the first question, we considered two persistence-only benchmarks: one based on the preceding June–May mean GMST and one based on the preceding May GMST value. To address the second and third questions, we used NMME multi-model-mean forecasts of December Niño-3.4 and monthly GMST.

To compare the simplified regression model with the NMME forecasts, we looked at trends and the relation in the models of December Niño-3.4 with GMST level and GMST-DC-PC1. The NMME models broadly reproduce the observed ENSO–GMST relationships, although with notable model differences (Fig. S3; Table S5). Several models have GMST trends that are significantly larger than observed, as noted previously (DelSole et al., 2025; Swart et al., 2019; Tippett & Becker, 2024). For the correlation between GMST level and December Niño-3.4, CanESM5 and GEM5.2-NEMO are stronger than observed (Fig. S3). These two models also have the most positive December Niño-3.4 trends (Table S5). The COLA-RSMAS-CCSM4 GMST-Niño-3.4 correlation is weaker than observed, while the remaining models are close to observations. For the relation between GMST-DC-PC1 and December Niño-3.4, COLA-RSMAS-CCSM4 is again much weaker than observed ( $r = 0.20$  compared with  $r = 0.62$ ). The remaining model correlations are slightly weaker than observed, with the exception of NCEP-CFSv2.

We next assessed performance relative to the persistence-only benchmarks. Both the simplified regression model and the NMME forecasts outperform the prior June–May mean benchmark in every month, as measured by RMSE (Fig. 4a). The May-value benchmark is more competitive early in the June–May year, particularly in June and July. Compared with this benchmark, both the simplified model and the NMME forecasts have lower RMSE from August through May. For the simplified regression model, there is little difference between using observed December Niño-3.4 and using forecast December Niño-3.4, and the RMSE differences are statistically insignificant in most months (Table S6). The NMME forecasts of GMST have lower RMSE than the simplified model for target months June through December, and similar RMSE for later target months. The largest

288 NMME advantage occurs in October, and the RMSE difference between the NMME GMST  
289 forecast and the simplified model using forecast December Niño-3.4 is statistically sig-  
290 nificant (Table S6). We computed MSESS using the prior June–May GMST average as  
291 the reference forecast (Fig. 4b). The resulting scores show that the simplified model im-  
292 proves most on persistence after December, consistent with the delayed GMST response  
293 to ENSO. In contrast, the NMME GMST forecasts show their largest advantage over  
294 persistence before December, especially in September and October.

295 Representative years illustrate these differences (Figs. 4c–h). In cool ENSO years,  
296 the simplified model captures the winter cooling and spring rebound but with reduced  
297 amplitude, as expected from regression shrinkage. In warm ENSO years, it captures de-  
298 layed warming, while the NMME forecasts are often closer to the observed level, espe-  
299 cially in 2015–16 and 2023–24. The 2023–24 case warrants particular attention. First,  
300 it was at least partly predictable because the NMME captures much of the observed warm-  
301 ing. Second, the role of El Niño is unclear since the ENSO-based forecast fails to repro-  
302 duce the June–November observed anomaly amplitude, and the September warming is  
303 not at the typical time when ENSO signals appear (Raghuraman et al., 2024; Rantanen  
304 & Laaksonen, 2024).

#### 305 **4 Summary and discussion**

306 Here we developed a simple and interpretable regression model that quantifies the  
307 relationship between ENSO and global mean surface temperature (GMST). The model  
308 allows the June–May evolution of monthly GMST to be anticipated based on informa-  
309 tion that is available near the beginning of June. We began with a high-dimensional for-  
310 mulation and applied a sequence of systematic, physically motivated simplifications to  
311 obtain a model with two predictors. The resulting predictors—recent GMST level and  
312 expected December Niño-3.4 value—serve to model the persistence of GMST and its de-  
313 layed response to ENSO. Principal component analysis (PCA) of 12-month June–May  
314 trajectories of GMST and Niño-3.4 was especially useful because the first two PCs of GMST  
315 and Niño-3.4 explain more than 95% of the variance of June–May trajectories. The ef-  
316 ficiency of PCA in explaining GMST evolution might be expected because a substan-  
317 tial fraction of GMST variance is associated with the long-term trend. The result is more  
318 striking for Niño-3.4 evolution, since a common view is that each ENSO event has its  
319 own distinct temporal structure.

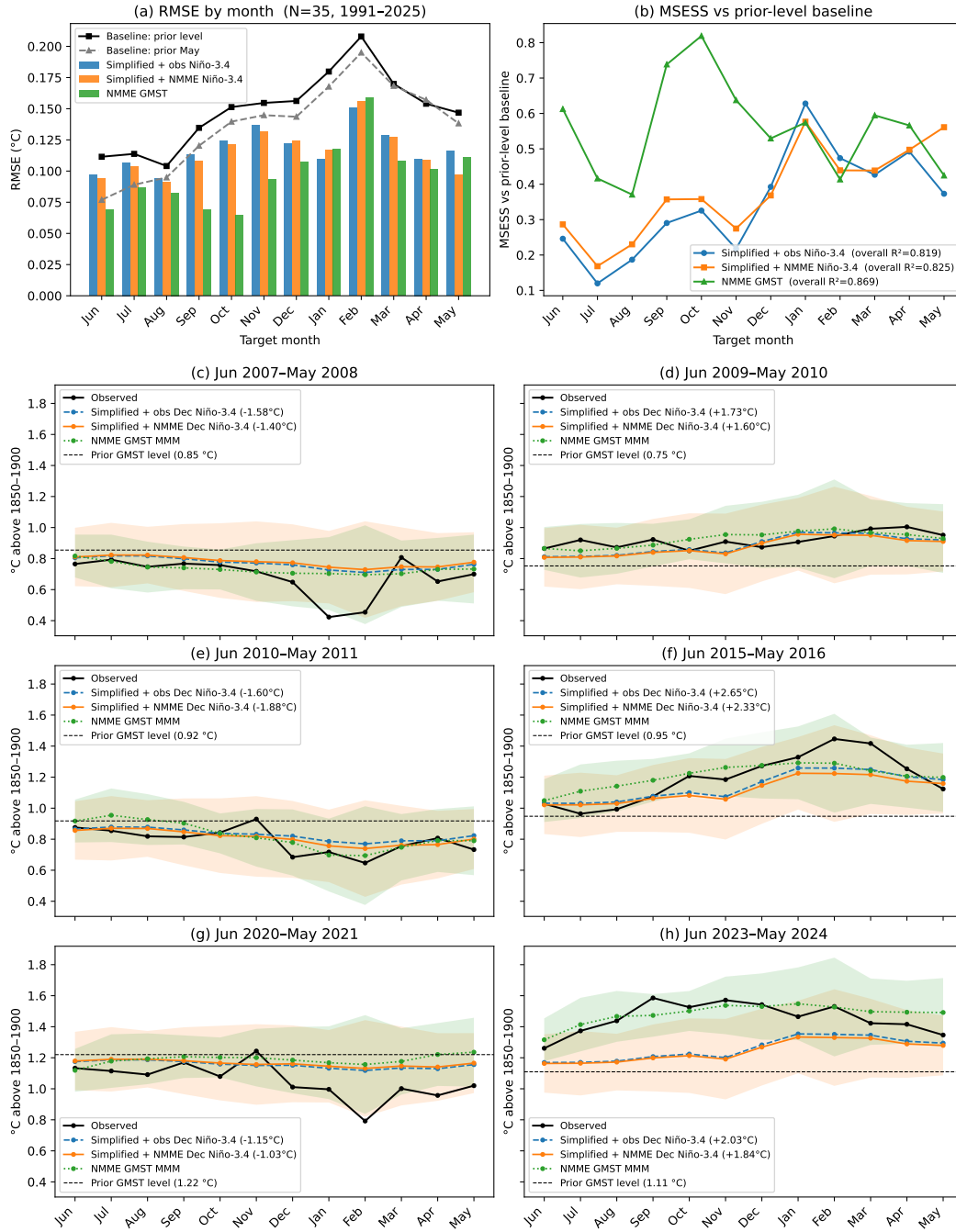


**Figure 4.** (a) Root-mean-squared error (RMSE) of the persistence baselines, the simplified model (using observed and forecast December Niño-3.4), and NMME forecasts of June–May global mean surface temperature (GMST) 1991–2026. (b) Mean-squared-error skill score (MSESS) of the simplified model and NMME forecasts relative to the prior June–May GMST level persistence baseline. Observed June–May GMST, simple model fits, and NMME GMST forecasts for (c) 2007–08, (d) 2009–10, (e) 2010–11, (f) 2015–16, (g) 2020–21, and (h) 2023–24. The simplified model inputs: observed and NMME-forecast Niño-3.4 values and prior GMST level are given in parenthesis. Shading as in Fig. 3e.

320 The structure of the leading EOFs suggested further simplifications to improve in-  
321 terpretability. Since the leading EOF of GMST is nearly uniform across months, GMST-  
322 PC1 was replaced by the June–May average of GMST. The leading Niño-3.4 EOF rep-  
323 represents the typical temporal evolution of ENSO and peaks in December, so the corre-  
324 sponding PC was replaced by the December value of Niño-3.4. These changes simplified  
325 the predictors with little loss of accuracy. According to the model, an expected Decem-  
326 ber Niño-3.4 anomaly of  $1^{\circ}\text{C}$  is associated with a GMST increase of about  $0.03^{\circ}\text{C}$  dur-  
327 ing June–August and a peak increase of about  $0.11^{\circ}\text{C}$  in the following February.

328 Although the ENSO contribution to GMST is modest, including ENSO improves  
329 prediction relative to persistence-only benchmarks. The simplified model reduces RMSE  
330 relative to the prior June–May mean benchmark in every month and relative to the prior  
331 May benchmark from August through May. The MSESS results show that this improve-  
332 ment is largest after December, consistent with the delayed GMST response to ENSO.  
333 Replacing observed December Niño-3.4 with forecast December Niño-3.4 produces lit-  
334 tle change in RMSE. By contrast, direct NMME forecasts of GMST show their largest  
335 advantage earlier in the June–May year, especially before December.

336 A broader implication is that ENSO information is most useful for GMST predic-  
337 tion when the forecast target is aligned with the ENSO life cycle. Calendar-year and annual-  
338 to-decadal forecast systems are valuable, but their initialization and verification windows  
339 are not optimized for taking advantage of post-spring-barrier ENSO predictability to an-  
340 ticipate June–May GMST evolution (Hermanson et al., 2022; World Meteorological Or-  
341 ganization, 2025; Dunstone et al., 2024; Folland et al., 2025). Initialized seasonal fore-  
342 cast systems, because they are run monthly, are better positioned to exploit the ENSO  
343 signal as it emerges and becomes reliable, although they still have known trend and ensemble-  
344 calibration errors (L’Heureux et al., 2022; Mayer et al., 2025; Tippett & Becker, 2024).  
345 Despite these limitations, the NMME multimodel mean provides a useful benchmark here  
346 and added skill relative to the simplified regression model during the early part of the  
347 June–May forecast year.

## Open Research Section

NOAAGlobalTemp version 6.1 data are available from Huang et al. (2026). NOAA Extended Reconstructed SST V5 (ERSSTv5) data are available from Huang et al. (2017b). Monthly values of the relative Niño-3.4 index are available from NOAA Climate Prediction Center (2026). NMME data are available from Tippett (2026).

## Conflict of Interest

The authors declare no conflicts of interest.

## Acknowledgments

We thank Michelle L. L'Heureux for helpful discussions and suggestions and two anonymous reviewers for their useful comments. Support from NSF is acknowledged by EJB (2223262). The authors also acknowledge the use of AI tools, including OpenAI's ChatGPT and Anthropic's Claude, to assist with code and manuscript editing.

## References

- Alexander, M. A., Bladé, I., Newman, M., Lanzante, J. R., Lau, N.-C., & Scott, J. D. (2002). The atmospheric bridge: The influence of ENSO teleconnections on air—sea interaction over the global oceans. *Journal of Climate*, *15*, 2205–2231. doi: 10.1175/1520-0442(2002)015<2205:TABTIO>2.0.CO;2
- Angell, J. K. (1981). Comparison of variations in atmospheric quantities with sea surface temperature variations in the equatorial eastern Pacific. *Monthly Weather Review*, *109*, 230–243. doi: 10.1175/1520-0493(1981)109<0230:COVIAQ>2.0.CO;2
- Angell, J. K. (2000). Tropospheric temperature variations adjusted for El Niño, 1958–1998. *Journal of Geophysical Research: Atmospheres*, *105*, 11841–11849. doi: 10.1029/2000JD900044
- Barnston, A. G., Tippett, M. K., Ranganathan, M., & L'Heureux, M. L. (2019). Deterministic skill of ENSO predictions from the North American Multimodel Ensemble. *Clim. Dyn.*, *53*, 7215–7234. doi: 10.1007/s00382-017-3603-3
- Becker, E. J., Kirtman, B. P., L'Heureux, M., Muñoz, Á. G., & Pegion, K. (2022). A decade of the North American Multimodel Ensemble (NMME): Research, application, and future directions. *Bulletin of the American Meteorological*

- 378           *Society*, 103, E973–E995. doi: 10.1175/BAMS-D-20-0327.1
- 379 Bunge, L., & Clarke, A. J. (2009). A verified estimation of the El Niño index Niño-  
380           3.4 since 1877. *Journal of Climate*, 22, 3979–3992. doi: 10.1175/2009JCLI2724  
381           .1
- 382 DelSole, T., & Tippett, M. K. (2014). Comparing forecast skill. *Monthly Weather*  
383           *Review*, 142, 4658–4678. doi: 10.1175/MWR-D-14-00045.1
- 384 DelSole, T., Tippett, M. K., & Johnson, N. C. (2025). Diagnosing errors in cli-  
385           mate forecast models using forced autoregressive models. *Journal of Advances*  
386           *in Modeling Earth Systems*, 17, e2024MS004926. doi: 10.1029/2024MS004926
- 387 DelSole, T. M., & Tippett, M. K. (2022). *Statistical methods for climate scientists*.  
388           Cambridge University Press. doi: 10.1017/9781108659055
- 389 Dunstone, N. J., Smith, D. M., Atkinson, C., Colman, A., Folland, C., Hermanson,  
390           L., . . . others (2024). Will 2024 be the first year that global temperature  
391           exceeds 1.5°C? *Atmospheric Science Letters*, 25, e1254.
- 392 Folland, C., Colman, A., Dunstone, N., Smith, D., & Scaife, A. (2025). A review  
393           of 25 annual forecasts of global mean surface temperature including the record  
394           warm years 2023 and 2024. *Geophysical Research Letters*, 52, e2025GL117308.  
395           doi: 10.1029/2025GL117308
- 396 Foster, G., & Rahmstorf, S. (2011). Global temperature evolution 1979–2010. *Envi-*  
397           *ronmental Research Letters*, 6, 044022. doi: 10.1088/1748-9326/6/4/044022
- 398 Glahn, H. R., & Lowry, D. A. (1972). The use of model output statistics (MOS) in  
399           objective weather forecasting. *J. Appl. Meteor.*, 11, 1203–1211.
- 400 Hermanson, L., Smith, D., Seabrook, M., Bilbao, R., Doblas-Reyes, F., Eti-  
401           enne Tourigny, V. L., . . . Kumar, A. (2022). WMO global annual to decadal  
402           climate update: a prediction for 2021–25. *Bulletin of the American Meteorolog-*  
403           *ical Society*, 103, E1117–E1129.
- 404 Huang, B., Thorne, P. W., Banzon, V. F., Boyer, T., Chepurin, G., Lawrimore,  
405           J. H., . . . Zhang, H.-M. (2017a). Extended reconstructed sea surface tem-  
406           perature, version 5 (ERSSTv5): Upgrades, validations, and intercomparisons.  
407           *Journal of Climate*, 30, 8179–8205. doi: 10.1175/JCLI-D-16-0836.1
- 408 Huang, B., Thorne, P. W., Banzon, V. F., Boyer, T., Chepurin, G., Lawrimore,  
409           J. H., . . . Zhang, H.-M. (2017b). NOAA Extended Reconstructed Sea Sur-  
410           face Temperature (ERSST), Version 5 [Dataset]. NOAA National Centers for

- 411 Environmental Information. doi: 10.7289/V5T72FNM
- 412 Huang, B., Yin, X., Menne, M. J., Vose, R., & Zhang, H.-M. (2022). Improvements  
413 to the land surface air temperature reconstruction in NOAAGlobalTemp: An  
414 artificial neural network approach. *Artificial Intelligence for the Earth Sys-*  
415 *tems*, 1, e220032. doi: 10.1175/AIES-D-22-0032.1
- 416 Huang, B., Yin, X., Menne, M. J., & Vose, R. S. (2026). NOAA Global Surface  
417 Temperature Dataset (NOAAGlobalTemp), Version 6.1 [Dataset]. NOAA Na-  
418 tional Centers for Environmental Information. doi: 10.25921/vvaa-wq11
- 419 Keith-Lucas, S. (2026, 10). *Is a ‘Super El Niño’ on the way and how will it af-*  
420 *fect the UK?* Retrieved from [https://www.bbc.com/weather/articles/](https://www.bbc.com/weather/articles/cj94nzzj33m0o)  
421 [cj94nzzj33m0o](https://www.bbc.com/weather/articles/cj94nzzj33m0o) (Accessed 2026-04-14)
- 422 Kirtman, B., Min, D., Infanti, J. M., Kinter, J. L., III, Paolino, D. A., Zhang, Q., ...  
423 Wood, E. F. (2014). The North American Multi-Model Ensemble (NMME):  
424 Phase-1 seasonal to interannual prediction, Phase-2 toward developing intra-  
425 seasonal prediction. *Bulletin of the American Meteorological Society*, 95,  
426 585–601. doi: 10.1175/BAMS-D-12-00050.1
- 427 Klein, S. A., Soden, B. J., & Lau, N.-C. (1999). Remote sea surface temperature  
428 variations during ENSO: Evidence for a tropical atmospheric bridge. *Journal*  
429 *of Climate*, 12, 917–932. doi: 10.1175/1520-0442(1999)012<0917:RSSTVD>2.0  
430 .CO;2
- 431 Klein, W. H., Lewis, B. M., & Enger, I. (1959). Objective prediction of five-day  
432 mean temperatures during winter. *Journal of Atmospheric Sciences*, 16, 672–  
433 682. doi: 10.1175/1520-0469(1959)016<0672:OPOFDM>2.0.CO;2
- 434 Lean, J. L., & Rind, D. H. (2008). How natural and anthropogenic influences alter  
435 global and regional surface temperatures: 1889 to 2006. *Geophysical Research*  
436 *Letters*, 35. doi: 10.1029/2008GL034864
- 437 L’Heureux, M. L., Levine, A., Newman, M., Ganter, C., Luo, J.-J., Tippett, M. K.,  
438 & Stockdale, T. (2020). ENSO Prediction. In M. McPhaden, A. Santoso, &  
439 W. Cai (Eds.), *El Niño-Southern Oscillation (ENSO) in a Changing Climate*.  
440 AGU. doi: 10.1002/9781119548164.ch10
- 441 L’Heureux, M. L., Tippett, M. K., & Wang, W. (2022). Prediction challenges from  
442 errors in tropical Pacific sea surface temperature trends. *Frontiers in Climate*,  
443 4. doi: 10.3389/fclim.2022.837483

- 444 L'Heureux, M. L., Tippett, M. K., Wheeler, M. C., Nguyen, H., Narsey, S., Johnson,  
445 N., . . . others (2024). A relative sea surface temperature index for classifying  
446 ENSO events in a changing climate. *Journal of Climate*, *37*, 1197–1211. doi:  
447 10.1175/JCLI-D-23-0406.1
- 448 Mayer, M., Balmaseda, M. A., Vitart, F., & Tietsche, S. (2025). Tropical Pacific  
449 trends in the ECMWF seasonal system and implications for predictions of  
450 the 2020–22 triple-dip La Niña. *Journal of Climate*, *38*, 2989–3003. doi:  
451 10.1175/JCLI-D-24-0467.1
- 452 NOAA Climate Prediction Center. (2026). Monthly Relative Niño-3.4 [Dataset].  
453 Retrieved from [https://www.cpc.ncep.noaa.gov/data/indices/Rnino34](https://www.cpc.ncep.noaa.gov/data/indices/Rnino34.ascii.txt)  
454 [.ascii.txt](https://www.cpc.ncep.noaa.gov/data/indices/Rnino34.ascii.txt)
- 455 Raghuraman, S. P., Soden, B., Clement, A., Vecchi, G., Menemenlis, S., & Yang,  
456 W. (2024). The 2023 global warming spike was driven by the El Niño–  
457 Southern Oscillation. *Atmospheric chemistry and physics*, *24*, 11275–11283.  
458 doi: 10.5194/acp-24-11275-2024
- 459 Rantanen, M., & Laaksonen, A. (2024). The jump in global temperatures in september  
460 2023 is extremely unlikely due to internal climate variability alone. *npj Climate and Atmospheric Science*, *7*, 34. doi: 10.1038/s41612-024-00582-9
- 462 Swart, N., Cole, J., Kharin, V., Lazare, M., Scinocca, J., Gillett, N., . . . Jiao, Y.  
463 (2019). The Canadian earth system model version 5 (CanESM5. 0.3). *Geoscientific Model Development*, *12*, 4823–4873. doi: 10.5194/gmd-12-4823-2019
- 465 Tippett, M. K. (2026). Data for: ENSO-conditioned evolution of global mean surface  
466 temperature [Dataset]. Zenodo. doi: 10.5281/zenodo.20514351
- 467 Tippett, M. K., & Becker, E. J. (2024). Trends, skill, and sources of skill in initial-  
468 ized climate forecasts of global mean temperature. *Geophysical Research Letters*, *51*, e2024GL110703. doi: <https://doi.org/10.1029/2024GL110703>
- 470 Tippett, M. K., & L'Heureux, M. L. (2020). Low-dimensional representations of  
471 Niño 3.4 evolution and the spring persistence barrier. *npj Climate and Atmospheric Science*, *3*, 24. doi: 10.1038/s41612-020-0128-y
- 473 Trenberth, K. E., Caron, J. M., Stepaniak, D. P., & Worley, S. (2002). Evolution  
474 of El Niño–Southern Oscillation and global atmospheric surface tempera-  
475 tures. *Journal of Geophysical Research: Atmospheres*, *107*, AAC–5. doi:  
476 10.1029/2000JD000298

- 477 Wilks, D. S. (2011). *Statistical methods in the atmospheric sciences: An introduc-*  
478 *tion*. Academic Press.
- 479 World Meteorological Organization. (2025, May 28). *WMO Global Annual to*  
480 *Decadal Climate Update 2025–2029*. Retrieved from [https://wmo.int/sites/](https://wmo.int/sites/default/files/2025-05/WMO_GADCU_2025-2029_Final.pdf)  
481 [default/files/2025-05/WMO\\_GADCU\\_2025-2029\\_Final.pdf](https://wmo.int/sites/default/files/2025-05/WMO_GADCU_2025-2029_Final.pdf) (Accessed 2026-  
482 04-18)
- 483 World Meteorological Organization. (2026, March). *ENSO neutral conditions ex-*  
484 *pected as La Niña fades, but El Niño chances rise*. [https://wmo.int/news/](https://wmo.int/news/media-centre/enso-neutral-conditions-expected-la-nina-fades-el-nino-chances-rise)  
485 [media-centre/enso-neutral-conditions-expected-la-nina-fades-el](https://wmo.int/news/media-centre/enso-neutral-conditions-expected-la-nina-fades-el-nino-chances-rise)  
486 [-nino-chances-rise](https://wmo.int/news/media-centre/enso-neutral-conditions-expected-la-nina-fades-el-nino-chances-rise). (Accessed: 2026-04-05)

487 **Supporting Information for “ENSO-conditioned evolution of global mean**  
488 **surface temperature”**

489 **Michael K. Tippett<sup>1</sup> and Emily J. Becker<sup>2</sup>**

490 <sup>1</sup>Department of Applied Physics and Applied Mathematics, Columbia University, New  
491 York, New York

492 <sup>2</sup>Rosenstiel School of Marine, Atmospheric, and Earth Science, University of Miami,  
493 Miami, Florida

494 **Contents of this file**

495 1. Figures S1 to S3

496 2. Tables S1 to S6

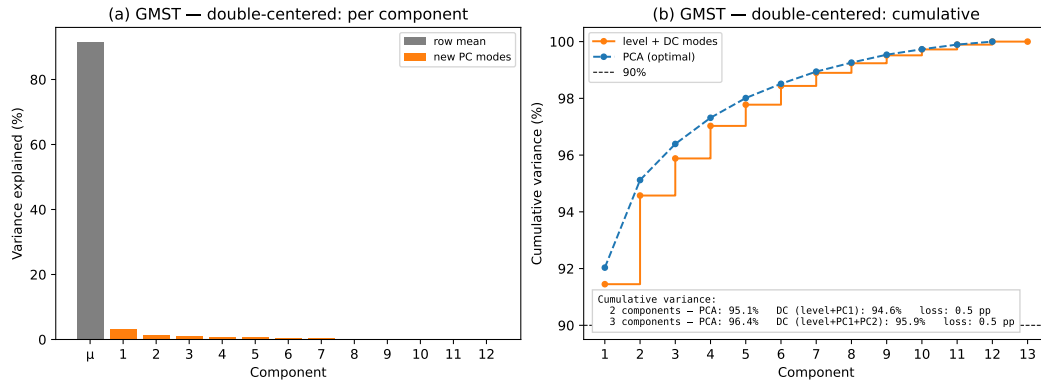


**Figure S1.** Variance per mode and cumulative variance for GMST double-centered PCA.

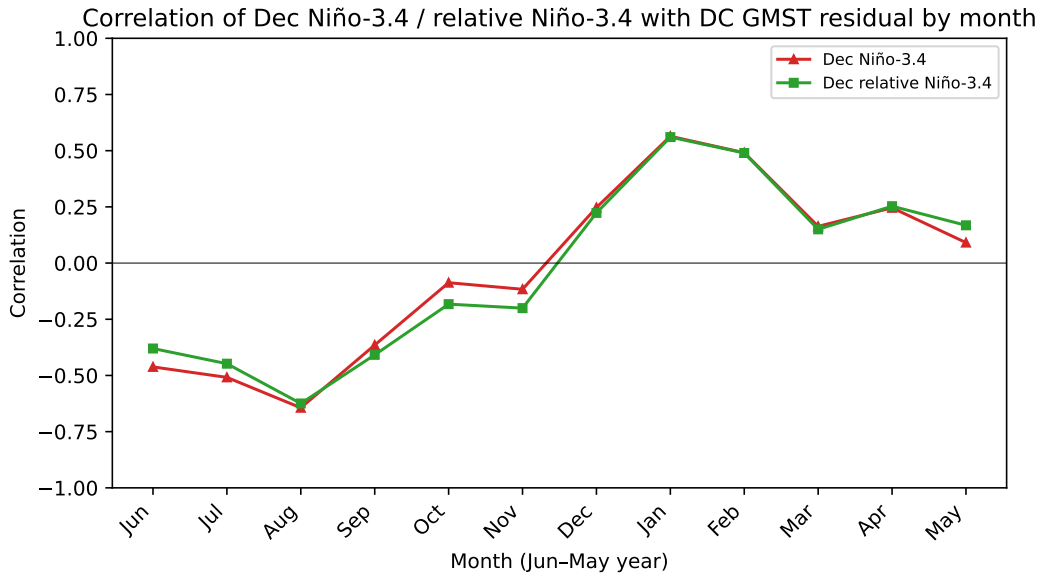


**Figure S2.** December Niño-3.4 and relative December Niño-3.4 correlations with DC GMST residuals (level removed) by month.

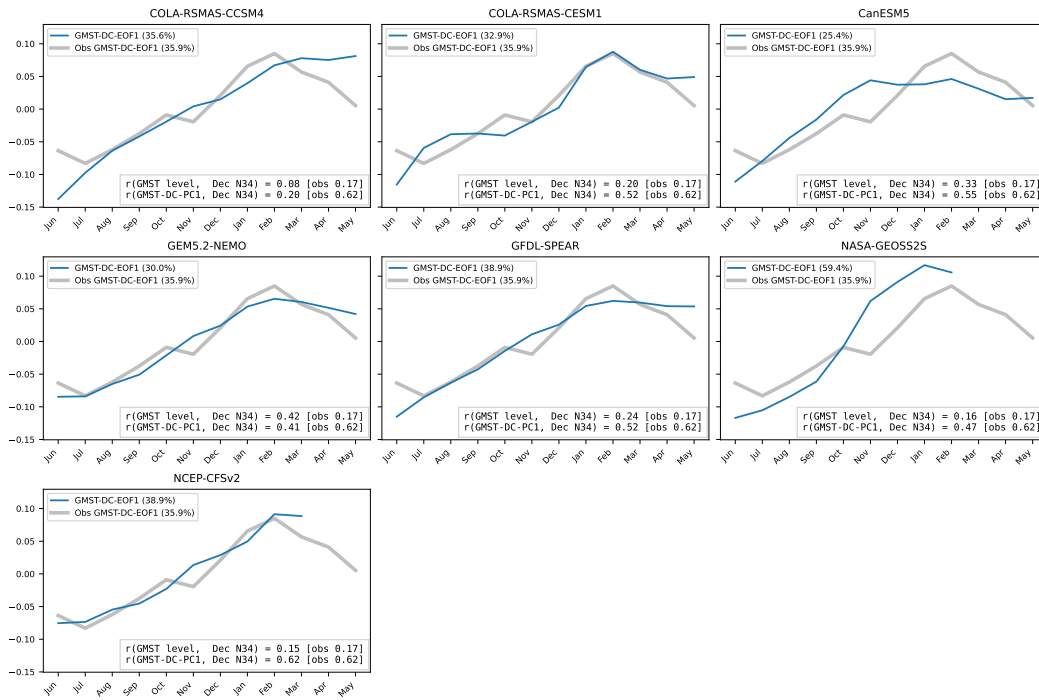


**Figure S3.** The first double-centered EOF of GMST (GMST-DC-EOF1) in seven NMME models and observations. The text box shows the correlation of the model's Niño-3.4 with the model's GMST level and DC-PC1. The observed values are in brackets for comparison.

	GMST-PC1( $t + 1$ )	GMST-PC2( $t + 1$ )
const	0.058 (0.042)	-0.023 (0.115)
GMST-PC1( $t$ )	0.979*** (0.044)	-0.118 (0.120)
GMST-PC2( $t$ )	-0.035 (0.042)	-0.177 (0.115)
N34-PC1( $t+1$ )	0.273*** (0.042)	0.594*** (0.116)
N34-PC2( $t+1$ )	-0.077* (0.042)	0.147 (0.116)
R-squared	0.927	0.444
R-squared Adj.	0.920	0.389
$N$	46	46

Standard errors in parentheses. \*  $p < .1$ , \*\*  $p < .05$ , \*\*\*  $p < .01$

**Table S1.** Regression results for the four-PC model

	GMST-PC1( $t + 1$ )	GMST-PC2( $t + 1$ )
const	0.059 (0.043)	-0.024 (0.118)
GMST-PC1( $t$ )	0.975*** (0.045)	-0.109 (0.123)
N34-PC1( $t+1$ )	0.272*** (0.043)	0.593*** (0.119)
R-squared	0.920	0.386
R-squared Adj.	0.916	0.357
$N$	46	46

Standard errors in parentheses. \*  $p < .1$ , \*\*  $p < .05$ , \*\*\*  $p < .01$

**Table S2.** Regression results for the two-PC model

	GMST mean( $t + 1$ )	DC-PC1( $t + 1$ )
const	0.018 (0.013)	-0.013 (0.118)
GMST mean( $t$ )	0.981*** (0.045)	0.097 (0.419)
Dec Niño-3.4( $t + 1$ )	0.066*** (0.011)	0.527*** (0.100)
R-squared	0.920	0.393
R-squared Adj.	0.916	0.364
$N$	46	46

Standard errors in parentheses. \*  $p < .1$ , \*\*  $p < .05$ , \*\*\*  $p < .01$

**Table S3.** Regression results for the simplified model.

	GMST mean( $t + 1$ )	DC-PC1( $t + 1$ )
const	0.019 (0.013)	-0.003 (0.118)
GMST mean( $t$ )	1.022*** (0.049)	0.472 (0.436)
Dec rel. Niño-3.4( $t + 1$ )	0.061*** (0.011)	0.523*** (0.100)
R-squared	0.909	0.389
R-squared Adj.	0.904	0.361
$N$	46	46

Standard errors in parentheses. \*  $p < .1$ , \*\*  $p < .05$ , \*\*\*  $p < .01$

**Table S4.** Regression results for the simplified model using relative Niño-3.4.

Model	GMST level (°C decade <sup>-1</sup> )	Dec Niño-3.4 (°C decade <sup>-1</sup> )
COLA-RSMAS-CCSM4	0.25 [0.21, 0.28]	-0.10 [-0.52, 0.32]
COLA-RSMAS-CESM1	0.35 [0.32, 0.38]	0.06 [-0.43, 0.57]
CanESM5	0.29 [0.26, 0.33]	0.18 [-0.04, 0.42]
GEM5.2-NEMO	0.23 [0.19, 0.28]	0.18 [-0.15, 0.55]
GFDL-SPEAR	0.32 [0.28, 0.36]	0.06 [-0.30, 0.45]
NASA-GEOSS2S	0.26 [0.22, 0.30]	-0.32 [-0.81, 0.25]
NCEP-CFSv2	0.27 [0.23, 0.32]	-0.15 [-0.61, 0.33]
Observations	0.24 [0.21, 0.28]	-0.09 [-0.45, 0.32]

**Table S5.** Trends for June starts over the period 1991–2026. The 95% confidence intervals are computed by block bootstrap sampling over start years.

	Jun	Jul	Aug	Sep	Oct	Nov	Dec	Jan	Feb	Mar	Apr	May
<i>Simplified + obs Niño-3.4 vs. Simplified + NMME Niño-3.4</i>												
Wilcoxon	0.27	0.32	0.11	<b>0.02</b>	0.40	0.61	0.89	0.18	0.93	0.73	0.69	<b>0.01</b>
Sign test	0.74	1.00	0.31	0.09	0.74	1.00	1.00	0.74	0.50	0.74	1.00	0.09
<i>Simplified + NMME Niño-3.4 vs. NMME GMST</i>												
Wilcoxon	<b>0.04</b>	0.67	0.68	0.40	< <b>0.01</b>	0.14	0.39	0.83	1.00	0.38	0.97	0.28
Sign test	0.50	1.00	1.00	0.31	< <b>0.01</b>	0.31	0.74	0.74	0.50	1.00	1.00	0.31

**Table S6.** Two-sided  $p$ -values for Wilcoxon signed-rank and sign tests per calendar month, 1991–2025 ( $N = 35$ ) for the difference in RMSE (top block) of the simple model using observed and NMME-forecast values of December Niño-3.4 and (bottom block) of the simple model using NMME-forecast values of December Niño-3.4 and direct NMME GMST forecasts. Bold font marks  $p \leq 0.05$ .